Spectroscopic and Judd-Ofelt Analysis of Nd3+ Ion Doped Lithium Antimony-Borate Glasses for Visible and Near Infrared Laser Application Compared to Standard Emission at 1.06 μm

M. Iezid, A. Abidi, F. Goumeidane, M. Poulain, M Legouera, P. Syam Prasad, P. Venkateswara Rao

Spectroscopic investigation and Judd-Ofelt analysis of Nd^{3+} doped lithium antimony-borate glasses

M. Iezid [a], A. Abidi [b], F. Goumeidane [c], M. Poulain [d], M. Legouera [e], P. Syam Prasad [f], P. Venkateswara Rao *[g]

[a] *Laboratoire d'Innovation en Construction, Eco-conception et Genie Sismique (LICEGS); University Mostafa Ben Boulaid Batna 2, Algeria.*

[b] *Laboratory of Organic Synthesis, Modeling and Optimization of Chemical Processes, Department of Process Engineering, University of Badji-Mokhtar, Annaba, 23000, Algeria.*

[c] *Laboratory of Active Components and Materials; Larbi Ben M'hidi University, Oum El Bouaghi, 04000, Algeria.*

[d] *Institut des Sciences Chimiques de Rennes, University Rennes 1, France.*

[e] *Laboratoire de Genie Mecanique et Materiaux; University 20 Aout 1955, Skikda, Algeria.*

[f] *Department of Physics, National Institute of Technology Warangal, Warangal 506004, Telangana, India*

[g] *Department of Physics, The University of the West Indies, Mona Campus, Jamaica.*

Abstract

The present work focuses on the spectroscopic luminescence analysis of trivalent neodymium-doped lithium antimony-borate glasses, with the glass composition 70 Sb_2O_3 – (25-x) B_2O_3 – 5 LiO_2 – x Nd_2O_3 where x= 0.3; 0.5; 0.7 mol. % (SBLN). Around 475 nm excitation used by the transition $^4I_{9/2} \rightarrow {}^2G_{9/2} + {}^2D_{3/2} + {}^2K_{15/2}$ and that induced emission lines of wavelengths λ_{emis}=584;673;767;826 nm (red is low intensity). The specific emission follows the transitions $^2G_{7/2} + {}^4G_{5/2} \rightarrow {}^4I_J$ (J=9/2; 11/2; 13/2; 15/2). Previous work on Nd^{3+} doped glasses studied near-infrared emission in $^4F_{3/2} \rightarrow {}^4I_J$ mode (J= 9/2; 11/2; 13/2) via near-infrared excitation $^4I_{9/2} \rightarrow {}^4F_{5/2} + {}^2H_{9/2}$.

The Judd-Ofelt analysis applied to SBLN glasses showed that the Ω_K parameters are consistent with the values in the literature. SBLN7 glass has the best spectroscopic factor Ω_4/Ω_6 = 0.974; while the best luminescence branching ratio is that of the green emission and it stands at an average β= 70%. The lifetimes are in the order of twenty microseconds. Similarly, green emission has the best values of stimulated emission cross section and gain

bandwidth. The chromatic coordinates showed accurately that the color itself lies in the yellowish-green region of the chromaticity diagram edited by CIE 1931. The calculation of its temperature was made by Mc Macy's equation, and it is in the limits of 5100 K; which corresponds to a cool color similar to midday sunlight.

Keywords: trivalent neodymium, glass, Judd-Ofelt parameters, emission cross-section, gain bandwidth, color coordinates.

***Corresponding author: P. Venkateswara Rao**

E-mail: pvrao54@gmail.com

1. Introduction

Glasses doped with trivalent lanthanides are widely applied in Photonics and Optronics technologies [1–4]. These materials took on the ultimate importance due to their attractive, functional properties, namely the possibility of generating high fluorescence intensity, a distributed lifetime from nano to milliseconds scale, and a good monochromatic aspect for a given transition [5]. The optimization of these properties requires the appropriate choice of the lanthanide including its concentration and its ligand, and thus the glassy matrix in which is incorporated [2].

The electronic transitions in the trivalent lanthanides are of the 4f–4f or 4f-5d type are mainly forced electrical in nature; their intensities can be determined via the Judd-Ofelt model [6, 7]. Magnetic transitions have a limited contribution and are governed by specific selection rules [8].

Trivalent lanthanides that can emit a wide range of spectrum in infrared and visible [9–14]; and often the evaluation of a given color is done in the BGR (Blue, Green, Red) system in terms of chromatic coordinates and appropriate temperature [15]. Neodymium is renowned for its infrared luminescence, and it is applied in telecommunications [5].

Heavy metal oxide glasses (HMOGs), in particular based on antimonate, are promising with respect to lanthanide doping. They exhibit low phonon energy, high refractive index and third-order nonlinear susceptibility [16–19].

The present work deals with the application of the Judd-Ofelt parameters for a neodymium-doped lithium Antimony-borate glasses (SBLN). Borate is added primarily to increase the solubility of neodymium in glass; since the reception capacity of lanthanides Ln^{3+} in antimonate matrices is low [20].

Previous work discussed on neodymium luminescence and has been focused on near-infrared emission of type $^4F_{3/2} \rightarrow {}^4I_J$ (J= 9/2; 11/2; 13/2; via near-infrared excitation $^4I_{9/2} \rightarrow {}^4F_{5/2} + {}^2H_{9/2}$ [2], [21–24].

In our case, we have presented another alternative to the study of the luminescence of Nd^{3+} incorporated in the lithium antimony-borate matrix; where we successfully detected four different green, red (low intensity), and two near-infrared emissions. These are luminescent transitions of type $^2G_{7/2} + {}^4G_{5/2} \rightarrow {}^4I_J$ (J= 9/2; 11/2; 13/2; 15/2) induced by an excitation in the visible according to $^4I_{9/2} \rightarrow {}^2G_{9/2} + {}^2D_{3/2} + {}^2K_{15/2}$.

The $^2G_{7/2} + {}^4G_{5/2}$ level is marked in the Dieke diagram [25] among the emissive levels of Nd^{3+} but the literature is of a low in the study of luminescent transitions starting from the orbital in question. The spectroscopic evaluation of the luminescence was made by calculating the spontaneous emission rate, the branching ratio and the lifetime. We determined the stimulated emission cross section via the Fuchtbauer-Landenburg formula [26] and the gain bandwidth coefficient. We also determined the x, y coordinates and the green color temperature using the emission spectra; then we represented the considered points in the chromaticity diagram published by CIE [27].

2. Experimental Methods

2.1. Synthesis of glasses

We opted for the choice of commercial chemicals of high purity for the synthesis of glassy samples such as $Sb_2O_3 \geq 99\%$ (Acros), $B_2O_3 \geq 99\%$ and $Li_2CO_3 \geq 99\%$ (Sigma Aldrich), Nd_2O_3 of 99.9% purity (Merck). The glass composition of the synthesized samples is glass composition 70 Sb_2O_3 – (25-x) B_2O_3 – 5 LiO_2 – x Nd_2O_3 (x= 0.3; 0.5; 0.7 mol. %) and labelled as SBLN3, SBLN5 and SBLN7. The SBLN glasses have been produced using the conventional melt-quenching method. We used silica crucibles containing intimate mixtures of starting materials. The melting was done in an electric furnace at around 850°C and it continues until a transparent and homogeneous liquid is obtained; then the liquid was poured into brass molds preheated to around 200°C. After solidification; the samples were brought to the

furnace for annealing for 8 hours at 250°C. The samples were cut and optically polished to prepare them in dimensions of 15 X 10 X 3 mm.

2.2. Characterizations

The glass matrix is characterized by X-ray diffraction; using a Bruker D8 model. The X-radiation used comes from a copper anticathode with a wavelength of 1.54 A°, generated under a voltage of 40 KV and a current of 40 mA. The angle sweep is between 10 and 70°.

We used a Q 20 type DSC device with a sensitivity of 10^{-1} °C to determine the characteristic temperatures of the glass matrix at a rate of 10°C/min. The measurement uncertainty on the glass transition temperature T_g is ± 2°C and ±1°C for crystallization onset T_x and the peak temperature T_p. Argon was the medium in the furnace.

We measured the microhardness of the prepared samples with a Matsuzawa MXT 70 durometer type driven by a diamond pyramidal indenter (Vickers); where we selected a load of 100 grams force; which was applied to the sample for 10 seconds. The measurement of the diameter of the impression (in the shape of a lozenge) expressed in micrometers, is done by means of an optical device integrated into the device. The precision is in 10^{-2} µm order.

The density of the samples was measured by the Archimedes method; whose emersion liquid is distilled water. The measurement uncertainty equals 10^{-3} g/cm^3.

The measurement of the absorbance of the samples was made between 200 and 2000 nm; with a Perkin Elmer spectrophotometer model equipped with a TDS WB InGaAs detector; with a resolution ± 1 nm.

The measurement of the luminescence of the Nd^{3+} doped samples was made at room temperature, with 475 nm excitation wavelength via a Fluorolog FL 3 – 22 SPEX – Jobin – Yovan model fluorometer; and the light source is a 450 W Xenon arc lamp emitted between 200 and 900 nm. The sample is placed in a support made at an angle of 22.5° with respect to the incident light in order to avoid interference between the excitation and the emission light. The resolution is equal to ± 0.5 nm.

3. Results and interpretation

3.1. Characteristics of the vitreous matrix:

The glassy nature of the matrix was confirmed by X-ray diffraction and DSC differential scanning calorimetry. Fig.1 shows the amorphous halo recorded on the diffraction spectrum, and Fig.2 shows a typical thermogram of the glassy state; including the glass transition and the crystallization peak.

Table 1 reports some parameters of the pure glass sample SBL, namely the density, the microhardness, the characteristic temperatures (T_g, T_x and T_p) and the thermal stability.

The density is within the limits of HMOG glasses [18] and is governed by equation (1):

$$\rho = \frac{W_a}{W_a - W_b}\rho_x \qquad (1)$$

Such that W_a and W_b are the weights of the sample in air and in the emersion liquid (distilled water) respectively, while ρ_x the density of the emersion liquid.

The Vickers microhardness [28] is determined using equation (2):

$$H_V = 1.8544\ \frac{P}{d^2} \qquad (2)$$

Note that P is the load expressed in Kgf, and d the diameter of the indentation in mm; while H_V microhardness is in Kgf/mm^2.

We evaluated the stability according to the criterion expressed by equation (3):

$$\Delta T = T_X - T_g \qquad (3)$$

With T_X the crystallization onset temperature and T_g the glass transition temperature. We noted that the vitreous matrix has a good stability where ΔT=135 K.

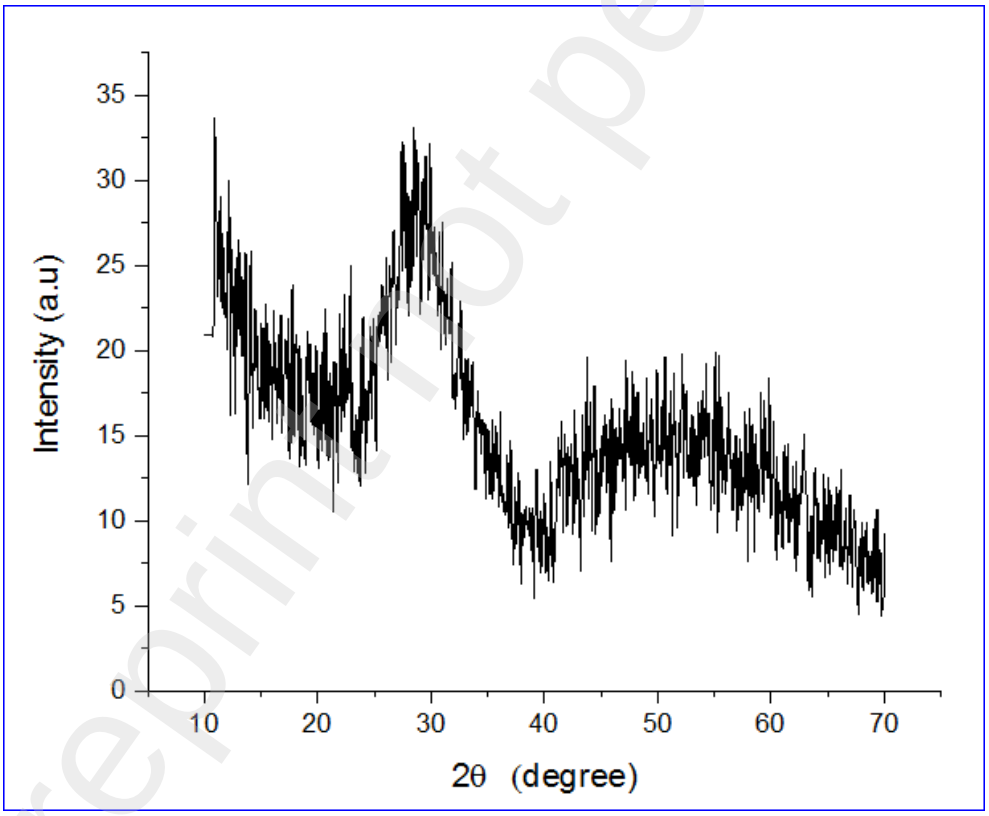

Fig. 1 Diffraction pattern of the SBL matrix; indicates the establishment of the amorphous state by the appearance of a halo (bump around 30°).

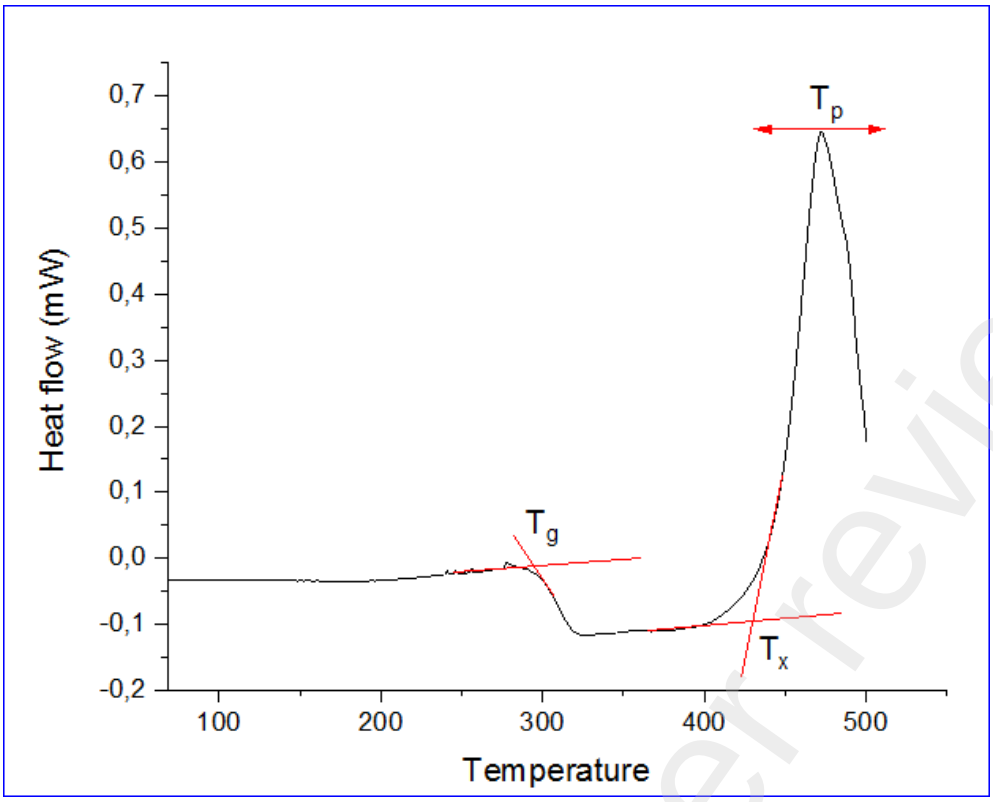

Fig. 2 DSC thermogram of the SBL matrix; indicating the glass transition T_g, the crystallization onset temperature T_x and the crystallization peak T_p.

Table 1. Some parameters of the pure SBL vitreous matrix

Density	microhardness	Characteristic temperatures			
Stability					
(g/cm^3)	(Kgf/mm^2)				(°C)
(K)					
		T_g	T_x	T_p	
4.537	203.5	295	430		465
135					

3.2. Optical absorption spectra and determination of refractive indices

The absorption spectra of the pure SBL matrix and the SBLN doped glasses are reported in Fig. 3. We have designated the absorption peaks recorded at room temperature between 400 and 900 nm; with $^4I_{9/2}$ is the ground state.

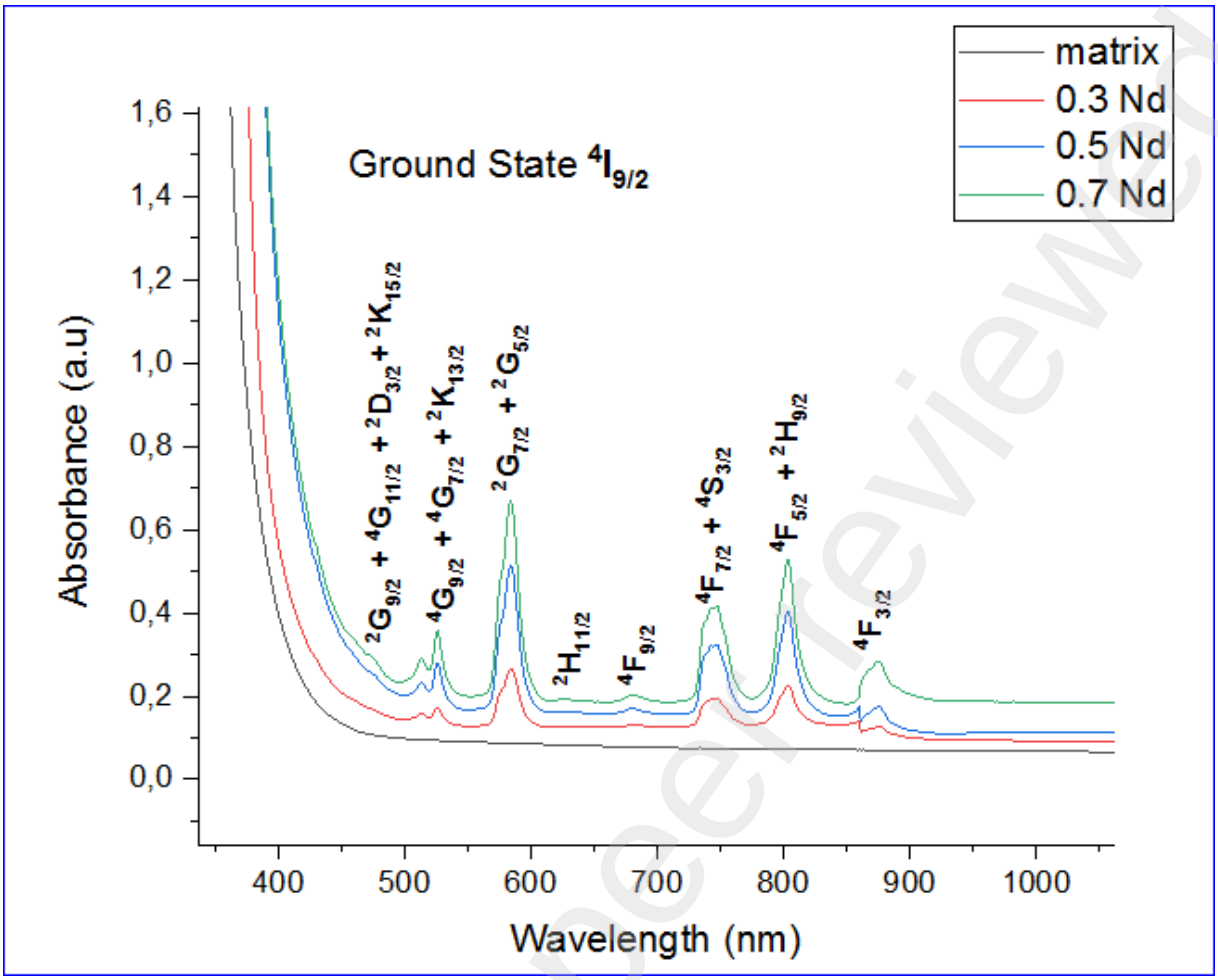

Fig. 3 Absorption spectra of the pure SBL matrix and the SBL neodymium doped glasses, where the different transitions refer to the ground state $^4I_{9/2}$

The refractive index was calculated using formula (4) of Dimitov and Sakka [29] according to:

$$\frac{n^2-1}{n^2+1} = 1 - \sqrt{\frac{E_g}{20}} \qquad (4)$$

Where E_g is the optical band gap expressed in eV; and we have determined it via the Tauc plot [30]; as shown in Fig. 4. The optical band gaps are obtained by the intersections of the tangents of the curves of the functions ν(αhν)=f(hν) with the abscissa axis (Fig.4) here α is the linear absorption coefficient; h is the Planck constant and ν is the frequency.

Table 2 summarizes the values of the optical band gaps as well as the refractive indices and the densities of the doped glasses.

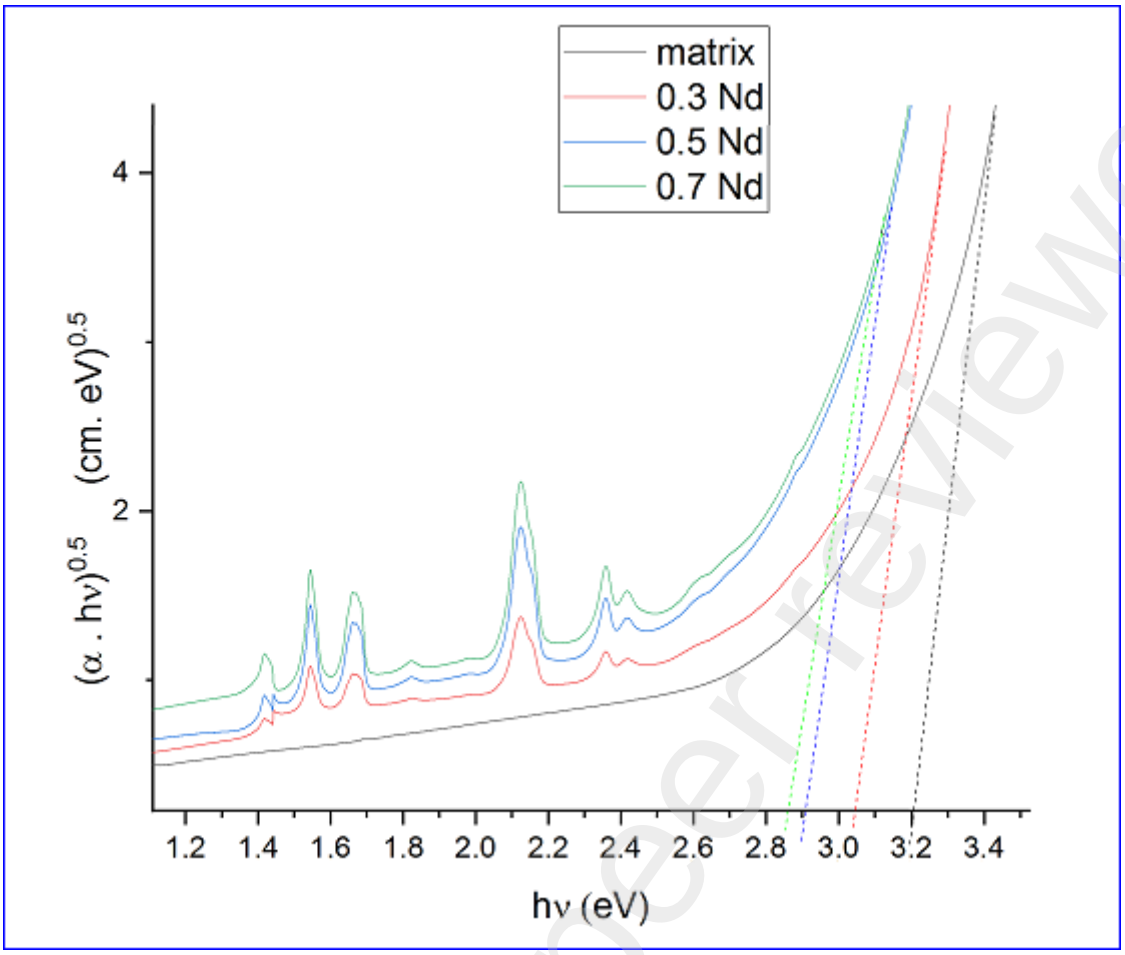

Fig. 4 Tauc plot for determining the optical band gaps of the pure SBL matrix and the SBL neodymium doped glasses.

Table 2. Density reports optical gap and refractive index

glass	Density (g/cm^3)	optical gap(eV)	refractive index
SBL (pure)	4.537	3.2	2.345
SBLN3	4.554	3.05	2.383
SBLN5	4.558	2.91	2.419
SBLN7	4.572	2.85	2.437

3.3 Judd-Ofelt analysis and luminescence study of SBLN glasses

The oscillator strength is calculated by the absorbance measurement data:

$$F_{exp} = \frac{2330\, mc^2}{\pi e^2 N_0} \int \varepsilon(\nu)\, d\nu \qquad (5)$$

Where m and e are the mass and charge of the electron, c the speed of light, N_0 the Avogadro number and ε(ν) the extinction coefficient which is determined with the Beer-Lambert law [31]:

$$\varepsilon(\nu) = \frac{\log\left(\frac{I_0}{I}\right)}{Cd} \qquad (6)$$

Where the absorbance $\log(I_0/I)$ measured as a function of wavenumber ν (cm^{-1}); C is the concentration of lanthanide in the sample (mol/L) and d is the thickness (cm).

According to the Judd-Ofelt theory [6], [7] the oscillator strength of a transformation $aJ \rightarrow bJ'$ is expressed by:

$$F_{cal} = F_{ed} + F_{md} = \frac{8\pi^2 mc\nu}{3h(2J+1)e^2 n^2}(\chi_{ed} S_{ed} + \chi_{md} S_{md}) \qquad (7)$$

Note that χ_{ed} and χ_{md} are given by:

$$\chi_{ed} = \frac{n(n^2+2)^2}{9} \qquad (8)$$

$$\chi_{md} = n^3 \qquad (9)$$

The electric and magnetic dipole line strengths are given by:

$$S_{ed}(aJ \rightarrow bJ') = e^2 \sum_{t=2,4,6} \Omega_t \left|\langle aJ \left| U^t \right| bJ' \rangle\right|^2 \qquad (10)$$

$$S_{md}(aJ \rightarrow bJ') = \frac{e^2}{4m^2c^2} \left|\langle aJ \left| L + 2S \right| bJ' \rangle\right|^2 \qquad (11)$$

Probable magnetic dipole transitions; are only those obeying the selection rule: ΔS = ΔL= 0, ΔJ = 0, ±1 and contributing to the oscillator strength. The Judd-Ofelt parameters are obtained by fitting in the least square sense of the experimental values of the oscillator strength using the equation 5. According to Carnall et al. [32], [33], the elements of the reduced matrix $\left|\langle aJ \left| U^t \right| bJ' \rangle\right|^2$ are independent of the choice of the vitreous matrix. The fitting precision is given by the formula:

$$\delta_{rms} = \sqrt{\frac{\sum_{i=1}^{N}\left(F_i^{exp} - F_i^{cal}\right)^2}{\sum_{i=1}^{N} F_{exp}^2}} \qquad (12)$$

Such that N is the number of transitions considered; and note that: N > 3.

The emission probability rate is calculated according to the equation:

$$A(aJ,bJ') = A_{ed} + A_{md} = \frac{64\pi^4\nu^3}{3h(2J+1)}\left(\chi_{ed}S_{ed} + \chi_{md}S_{md}\right) \qquad (13)$$

The luminescence branching ratio is expressed as follows:

$$\beta = A(aJ,bJ')/\sum_{bJ'} A(aJ,bJ') \qquad (14)$$

The lifetime is the inverse of the total probability rate:

$$\tau = 1/\sum_{bJ'} A(aJ,bJ') \qquad (15)$$

The stimulated emission cross section is given by [26]:

$$\sigma(J\rightarrow J') = \frac{\lambda^4}{8\pi c n^2 \Delta\lambda_{eff}} A(J\rightarrow J') \qquad (16)$$

$$\Delta\lambda_{eff} = \frac{1}{I_p}\int I(\lambda)d\lambda \qquad (17)$$

$\Delta\lambda_{eff}$ is the full width at half maximum (FWHM) of the emission peak; and the product $\Delta\lambda_{eff}$ $\sigma(J\rightarrow J')$ represents the gain bandwidth coefficient.

3.3.1 Determination of Judd-Ofelt parameters

We have determined the Judd-Ofelt parameters with the calculation of the experimental forces according to equation (5), assuming the elements of the reduced matrix [33] and the barycenters of the absorption peaks described in Table 3:

Table 3: Barycenters of the absorption peaks and the elements of the reduced matrix

From $^4I_{9/2}$	wavenumber (cm^{-1})	matrix elements		
		U_2^2	U_4^2	U_6^2
$^2K_{15/2}$, $^2G_{9/2}$, $^2D_{3/2}$, $^4G_{11/2}$	21007	0.001	0.0441	0.0364

$^2K_{13/2}$, $^4G_{7/2}$, $^4G_{9/2}$	1915	0.0664	0.218	0.1271
$^4G_{5/2}$, $^2G_{7/2}$	17135	0.9736	0.5941	0.0673
$^2H_{11/2}$	15940	0.0001	0.0027	0.0104
$^4F_{9/2}$	14652	0.0009	0.0092	0.0417
$^4F_{7/2}$, $^4S_{3/2}$	13411	0.001	0.0449	0.6597
$^4F_{5/2}$, $^2H_{9/2}$	12447	0.0102	0.2451	0.5124
$^4F_{3/2}$	11428	0	0.2293	0.0549

(The error made in determining the barycenters is ± 40 cm^{-1})

The Judd-Ofelt parameters (Ω_K X 10^{-20} cm^2) of the three glasses are as follows:

$$\text{SBLN3}\begin{cases}\Omega_2 = 2.33\\ \Omega_4 = 1.53\\ \Omega_6 = 1.98\end{cases};\qquad \text{SBLN5}\begin{cases}\Omega_2 = 2.15\\ \Omega_4 = 0.98\\ \Omega_6 = 2.12\end{cases};\qquad \text{SBLN7}\begin{cases}\Omega_2 = 2.55\\ \Omega_4 = 3.1\\ \Omega_6 = 3.18\end{cases}$$

These parameters are validated by small mean square error values between the experimental and theoretical forces (see Table 4). The comparison of the Ω_K parameters of the SBLN5 glass with the literature is shown in Table 5. The SBLN7 glass has the best spectroscopic factor Ω_4/Ω_6 =0.974.

Table 4: Experimental and theoretical oscillator strength values and the root mean square deviations for SBLN glasses.

Transition from $^4I_{9/2}$	Oscillator strength X10^{-8}					
	SBLN3		SBLN5		SBLN7	
	F_{cal}	F_{exp}	F_{cal}	F_{exp}	F_{cal}	F_{exp}
$^2K_{15/2}$, $^2G_{9/2}$, $^2D_{3/2}$, $^4G_{11/2}$	91.93	4.59	81.36	19.7	170.36	33.16
$^2K_{13/2}$, $^4G_{7/2}$, $^4G_{9/2}$	432.64	449	376.68	444	759.58	750.07
$^4G_{5/2}$, $^2G_{7/2}$	1685.43	1680	1476.8	1470	2416.3	2327
$^2H_{11/2}$	11.92	8.44	12.25	5.05	20.72	13.67
$^4F_{9/2}$	43.27	42.6	44.83	39.3	74.74	63.68
$^4F_{7/2}$, $^4S_{3/2}$	548.54	476	592.8	559	938.14	911.51
$^4F_{5/2}$, $^2H_{9/2}$	524.01	621	512.18	552	936.9	895.6
$^4F_{3/2}$	165.29	82.9	126.96	70.9	326.4	326.66
δ_{rms}	0.09		0.071		0.063	

Table 5: Comparison of Judd-Ofelt parameters (Ω_K X10^{-20} cm^2) of SBLN5 glass with the literature

glass	Ω_2	Ω_4	Ω_6	Ω_4/Ω_6	order
SBLN5 present work	2.15	0.98	2.12	0.45	$\Omega_2 > \Omega_6 > \Omega_4$
PZNd0.5	3.76	1.16	3.23	0.36	$\Omega_2 > \Omega_6 > \Omega_4$ [3]
TBZNNd0.5	2.89	1.35	1.59	0.85	$\Omega_2 > \Omega_6 > \Omega_4$ [21]

0.5Nd PTR	3.65	2.95	3.73	0.79	$\Omega_2 < \Omega_6 > \Omega_4$ [1]
GN050	4.27	4.49	4.21	1.04	$\Omega_2 < \Omega_6 < \Omega_4$ [5]

3.3.2. Radiative properties of SBLN glasses

As we have already mentioned; the work presented in the literature, reporting the luminescence of Nd^{3+} in different vitreous matrices, focused on the near infrared emission $^4F_{3/2} \rightarrow {}^4I_J$ (J= 9/2; 11/2; 13/2); via an excitation $^4I_{9/2} \rightarrow {}^4F_{5/2} + {}^2H_{9/2}$. This corresponds to emissions close to λ_{emis}= 900; 1060; 1330 nm via an excitation of the order of λ_{exc}= 800 nm.

Our work is distinguished by a shorter excitation λ_{exc}=475 nm ($^4I_{9/2} \rightarrow {}^2G_{9/2} + {}^4G_{11/2} + {}^2D_{3/2} + {}^2K_{15/2}$) applied to SBLN glasses; which generated two visible green and red emissions (low intensity), and two near infrared emissions. These are the wavelengths around λ_{emis} = 584; 673; 767; 826 nm corresponding to the transitions $^2G_{7/2} + {}^4G_{5/2} \rightarrow {}^4I_J$ with J= 9/2; 11/2; 2/13; 15/2 (see Fig.5).

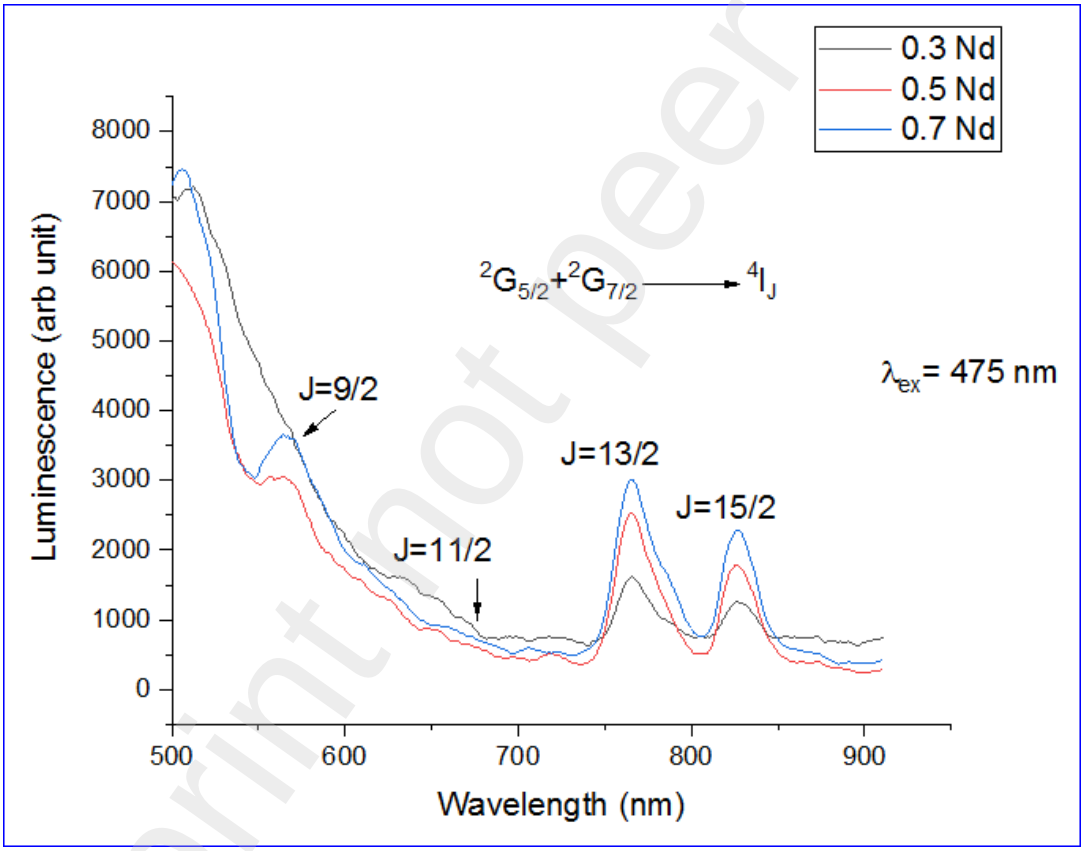

Fig. 5 Nd^{3+} emission spectrum of SBLN glasses recorded at room temperature with excitation wavelength λ_{exc}=475 nm and induced emissions are λ_{emis}=584; 675; 765; 827nm.

We calculated the spectroscopic parameters of these luminescent transitions using equations 13, 14 and 15. The results are summarized in Table 6 in terms of spontaneous emission rate A, branching ratio β and lifetime τ. We note that the green emission $^2G_{7/2}$ +

$^4G_{5/2} \rightarrow {}^4I_{9/2}$ has the best branching ratio which marks an average β =70%. Similarly, we calculated the stimulated emission cross section and the gain factor ($\Delta\lambda_{eff}$ σ) based on the emission spectrum of each glass (see Table 7). Then green emission has the best stimulated emission cross section and the highest gain coefficient.

The energy diagram (Fig.6) explains the mechanism driving the Nd^{3+} emission lines in the lithium Antimony –borate matrix. First, excitation around 475 nm promotes an electron from the ground state to the excited state according to:

$^4I_{9/2} \rightarrow {}^2G_{9/2} + {}^4G_{11/2} + {}^2D_{3/2} + {}^2K_{15/2}$ (GSA) ;

Then a multiphonon relaxation (non-radiative transition) takes place:

$^2G_{9/2} + {}^4G_{11/2} + {}^2D_{3/2} + {}^2K_{15/2} \rightarrow {}^2G_{7/2} + {}^4G_{5/2}$ (NR).

From the emissive level ($^2G_{7/2} + {}^4G_{5/2}$), it triggered four radiative transitions (R):

$^2G_{7/2} + {}^4G_{5/2} \rightarrow {}^4I_J$ (R) (J= 9/2; 11/2; 13/2; 15/2).

Note that the red transition corresponding to J = 11/2 is of low intensity; this is probably due to the hydroxyl group OH- which was inserted into the glasses during the synthesis. On the other hand, cross-relaxation (CR); is a non-radiative process can occur in SBLN glasses through the following transitions:

$(^2G_{7/2} + {}^4G_{5/2} ; {}^4I_{9/2}) \rightarrow ({}^4F_{7/2} + {}^4S_{3/2} ; {}^4I_{13/2})$ (CR)

$(^2G_{7/2} + {}^4G_{5/2} ; {}^4I_{9/2}) \rightarrow ({}^4F_{5/2} + {}^2H_{9/2} ; {}^4I_{15/2})$ (CR)

Table 6: Spectroscopic parameters for $^2G_{7/2} + {}^4G_{5/2} \rightarrow {}^4I_J$ transitions (J= 9/2; 11/2; 13/2; 15/2) related to SBLN glasses.

Glass	$^2G_{5/2} + {}^2G_{7/2} \rightarrow$	ν (cm^{-1})	A (s^{-1})	β	τ (µs)
SBLN3	$^4I_{15/2}$	12091.9	396.66	0.013	
	$^4I_{13/2}$	13071.9	892.27	0.03	
	$^4I_{11/2}$	14814.8	6948.47	0.237	
	$^4I_{9/2}$	17123.2	21030.72	0.718	34.16
SBLN5	$^4I_{15/2}$		448.62	0.016	
	$^4I_{13/2}$		807.53	0.03	
	$^4I_{11/2}$		6163.49	0.232	
	$^4I_{9/2}$		19066.75	0.719	37.75
SBLN7	$^4I_{15/2}$		695.31	0.015	

	$^4I_{13/2}$	1772.95	0.038	
	$^4I_{11/2}$	11793.96	0.259	
	$^4I_{9/2}$	31262.5	0.686	21.96

Table 7: Stimulated emission cross section and the gain bandwidth factor $\Delta\lambda_{eff}\,\sigma$ (these two parameters are calculated based on the emission spectrum of each glass).

glass	$^2G_{5/2} + {}^2G_{7/2} \rightarrow$	λ_{em}(nm)	$\Delta\lambda_{eff}$ (nm)	σ (10^{-21} cm^2)	$\Delta\lambda_{eff}\,\sigma$ (10^{-27} cm^3)
SBLN3	$^4I_{13/2}$	766	21.1	3.41	7.17
	$^4I_{15/2}$	826	19.9	2.17	4.31
SBLN5	$^4I_{9/2}$	584	22	28.8	50.3
	$^4I_{13/2}$	765	25.3	2.48	6.27
	$^4I_{15/2}$	827	22.4	2.12	4.76
SBLN7	$^4I_{9/2}$	584	29.4	27.7	81.2
	$^4I_{13/2}$	765	26.2	5.17	13.6
	$^4I_{15/2}$	827	21.7	3.35	7.26

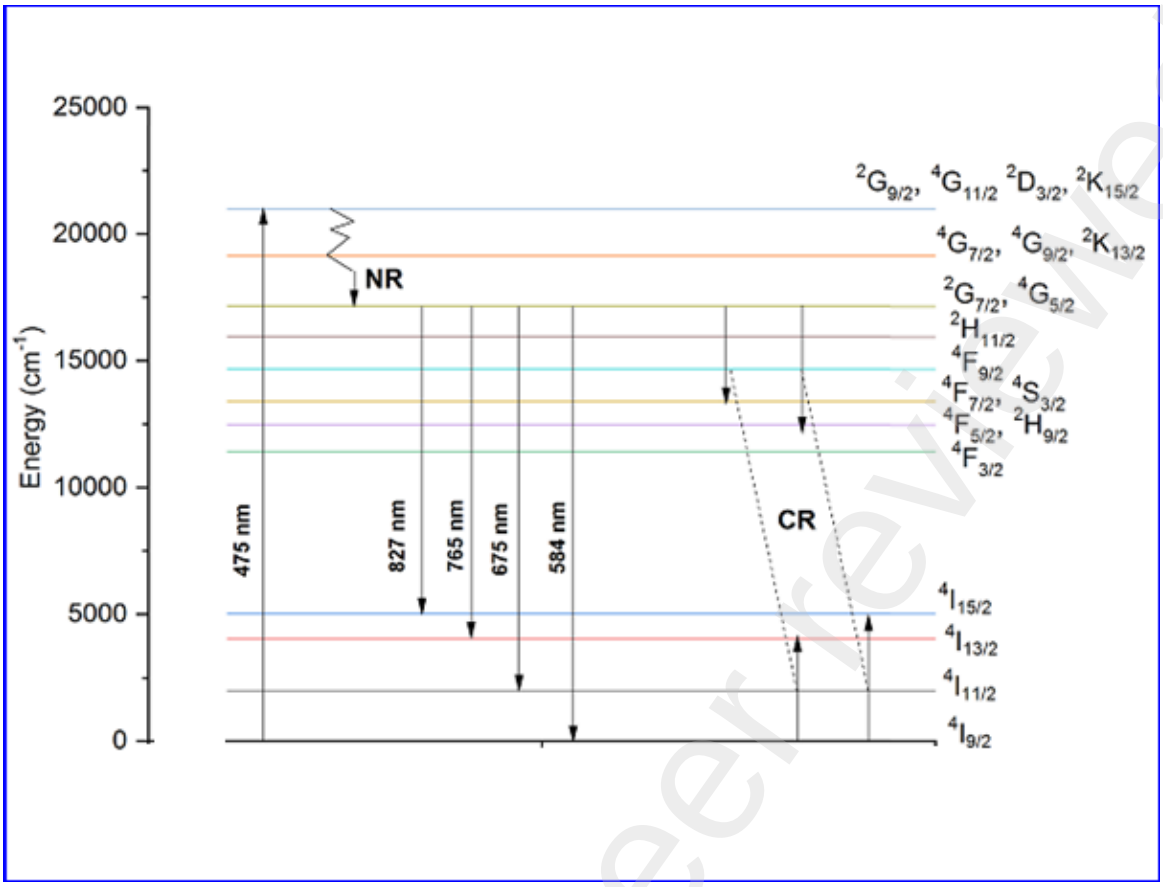

Fig. 6 Energy diagram explaining the emission of Nd^{3+} in the lithium antimony-borate glass matrix

3.3.3 Chromaticity coordinates and temperature of emitted green color

We calculated the x, y coordinates according to the procedure indicated by CIE; and we determined the correlated color temperature (CCT) through Mc Camy's formula [34] according to equation (18):

$$CCT = -449n^3 + 3525n^2 - 6823n + 5520.33 \qquad (18)$$

Such that $n = (x - x_e)/(y - y_e)$ is the inverse of the slope of a line and $(x_e = 0.332\ et\ y_e = 0.186)$ is the epicenter. These parameters are grouped together in Table 8. The coordinates associated with the SBLN5 and SBLN7 glasses are located in the yellowish-green region (Fig.7) and their CCTs are close to 5100 K indicating that these colors are qualified as cold and it is similar to sunlight at midday [27].

Table 8: Chromatic coordinates and CCT color temperature, SBLN5 and SBLN7 glasses

glass	coordinates		CCT (K)
	x	y	
SBLN5	0.3552	0.5968	5145.86

SBLN7	0.3573	0.593	5096.64

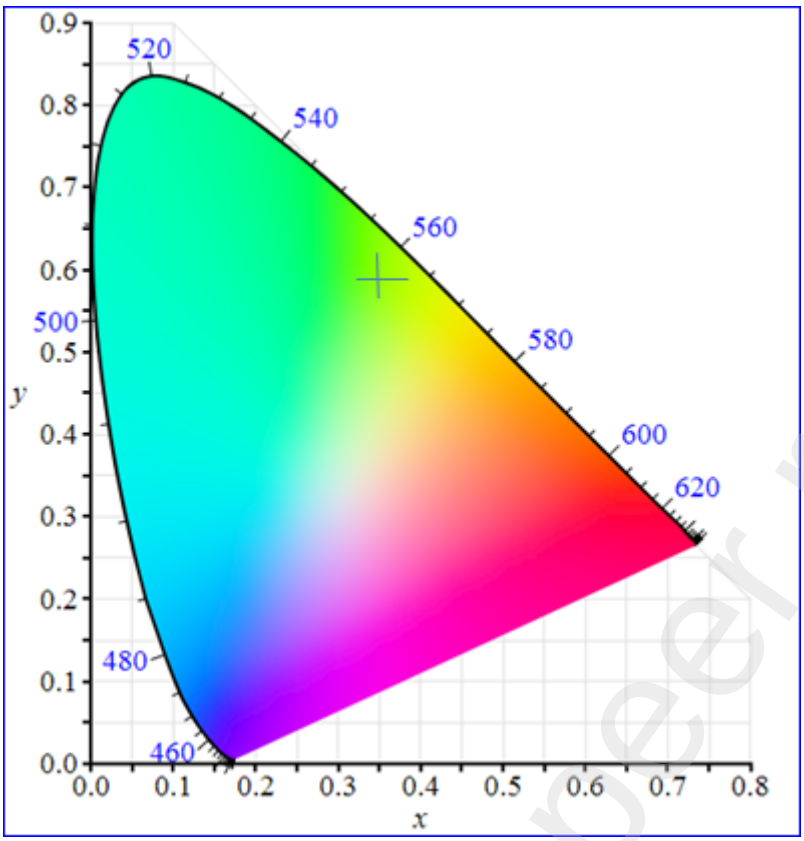

Fig. 7 Representation of chromatic coordinates of SBLN7 glass at intersection of vertical and horizontal lines in yellowish-green region of chromatic diagram (edited by CIE 1931).

Conclusion

This work concerns the study of the luminescence of trivalent neodymium doped lithium antimony-borate glasses 70 Sb_2O_3 – (25-x) B_2O_3 – 5 LiO_2 – x Nd_2O_3 (x= 0.3, 0.5, 0.7 mol %).

The vitreous state of the matrix was confirmed by X-ray diffraction (amorphous profile) and by DSC measurement. The glass transition temperature equals 295°C and the stability marked a good extent of ΔT equal 135 K. Also the density and Vickers microhardness of the matrix were reported.

The optical band gaps of the glasses were calculated by the Tauc method from the absorbance curves. These are used to determine the refractive indices of the pure and the doped glasses.

The Judd-Ofelt analysis shows that the Ω_K parameters of SBLN glasses are comparable to those published in the literature. In this context the spontaneous emission rate, the

branching ratio and the lifetime were calculated for the three glass samples SBLN3, SBLN5 and SBLN7. These calculations were made under the subject of the transitions recorded in the emission curves. However, the emissive transition of the green color has the best branching ratio at around 70%. The lifetimes are in the order of twenty microseconds. The emissive transitions themselves are of type $^2G_{7/2} + {}^4G_{5/2} \rightarrow {}^4I_J$ such that J =9/2, 11/2, 13/2, 15/2 corresponding to λ_{emis}=584; 675; 765; 827 nm. The excitation wavelength used is λ_{exc} = 475 nm and it is of type $^4I_{9/2} \rightarrow {}^2G_{9/2} + {}^4G_{11/2} + {}^2D_{3/2} + {}^2K_{15/2}$. The emission in visible and near infrared quality of SBLN glasses is explained by the energy diagram equipped with a diagram of excitation and emissions assisted by multiphonon relaxation and non-radiative processes such as cross-relaxation. The calculation of efficient stimulated emission cross-section and the gain bandwidth showed that the emission $^2G_{7/2} + {}^4G_{5/2} \rightarrow {}^4I_{9/2}$ has the best values; therefore we proceeded to the determination of these chromatic coordinates x, y using the emission curves of glasses doped with 0.5 and 0.7 mol.% Nd^{3+}. Then their coordinates lie in the yellowish-green region in the tristimulus diagram published by CIE and CCT temperatures close to 5100K indicate that the color quality is cold and that similar to sunlight at midday.

Bibliography

[1] K. Nasser, V. Aseev, S. Ivanov, A. Ignatiev, and N. Nikonorov, “Optical , spectroscopic properties and Judd – Ofelt analysis of Nd 3 + -doped,” *J. Lumin.*, vol. 213, no. May, pp. 255–262, 2019.

[2] X. Jiang, Y. Sun, X. Wang, L. Hu, S. Chen, and Q. Yang, “Spectroscopic properties and Stark splitting of Nd 3 + ions in different host glasses to obtain pure blue laser,” *J. Lumin.*, vol. 249, no. December 2021, p. 119005, 2022.

[3] Z. Ashur *et al.*, “Spectroscopic investigations of near-infrared emission from Nd 3 + -doped zinc-phosphate glasses : Judd-Ofelt evaluation,” *J. Non. Cryst. Solids*, vol. 509, no. May 2018, pp. 106–114, 2019.

[4] P. Thongyoy, C. Kedkaew, P. Meejitpaisan, P. H. Minh, and T. Keawmon, “Optik 1 . 06 µ m emission of Nd 3 + -doped aluminium barium lithium phosphate glasses for near IR laser medium material,” *Optik (Stuttg).*, vol. 269, no. August, p. 169852, 2022.

[5] X. Lin *et al.*, “Thermal and fluorescence properties of Nd 2 O 3 -doped Gd 2 O 3 -Ga 2 O 3 -GeO 2 glass based on the Judd-Ofelt theory,” *J. Non. Cryst. Solids*, vol. 594, no. July, p. 121810, 2022.

[6] G. S. Ofelt, “Intensities of crystal spectra of rare-earth ions,” *J. Chem. Phys.*, vol. 37, no. 3, pp. 511–520, 1962.

[7] B. R. Judd, “Optical absorption intensities of rare-earth ions,” *Phys. Rev.*, vol. 127, no. 3, p. 750, 1962.

[8] M. P. Hehlen, M. G. Brik, and K. W. Krämer, “50th anniversary of the Judd-Ofelt theory: An experimentalist’s view of the formalism and its application,” *J. Lumin.*, vol.

136, pp. 221–239, 2013.

[9] A. Jose, T. Krishnapriya, J. R. Jose, C. Joseph, and P. R. Biju, “Physica B : Physics of Condensed Matter NIR photoluminescent characteristics of Nd 3 + activated fluoroborosilicate glasses for laser material applications,” *Phys. B Phys. Condens. Matter*, vol. 634, no. November 2021, p. 413772, 2022.

[10] M. Iezid *et al.*, “Spectroscopic analysis of up conversion luminescence in doped halogeno-antimonite glass,” *Ceram. Int.*, vol. 44, no. 15, 2018.

[11] A. Jha *et al.*, “Rare-earth ion doped TeO 2 and GeO 2 glasses as laser materials,” *Prog. Mater. Sci.*, vol. 57, no. 8, pp. 1426–1491, 2012.

[12] A. Ichoja, S. Hashim, and S. K. Ghoshal, “Optik Judd − Ofelt calculations for spectroscopic characteristics of Dy 3 + - activated strontium magnesium borate glass,” *Opt. - Int. J. Light Electron Opt.*, vol. 218, no. June, p. 165001, 2020.

[13] H. Chen, F. Chen, T. Wei, Q. Liu, R. Shen, and Y. Tian, “Ho3+ doped fluorophosphate glasses sensitized by Yb3+ for efficient 2 μm laser applications,” *Opt. Commun.*, vol. 321, pp. 183–188, 2014.

[14] H. Ebendor and D. Ehrt, “Tb 3 f ± d absorption as indicator of the e ect of covalency on the Judd ± Ofelt X 2 parameter in glasses,” vol. 248, pp. 247–252, 1999.

[15] J. Schanda, *Colorimetry: understanding the CIE system*. John Wiley & Sons, 2007.

[16] M. Iezid *et al.*, “Judd-Ofelt analysis and luminescence studies of Er3+ doped halogeno-antimonate glasses,” *Opt. Mater. (Amst).*, vol. 120, p. 111422, 2021.

[17] F. Goumeidane, M. Legouera, M. Iezid, M. Poulain, V. Nazabal, and R. Lebullenger, “Synthesis and physical properties of glass in the Sb2O3-PbCl2-MoO3 system,” *J. Non. Cryst. Solids*, vol. 357, no. 21, pp. 3572–3577, 2011.

[18] M. Legouera, P. Kostka, and M. Poulain, “Glass formation in the Sb2O3–ZnBr2 binary system,” *J. Phys. Chem. Solids*, vol. 65, no. 5, pp. 901–906, 2004.

[19] M. Iezid, M. Legouera, F. Goumeidane, M. Poulain, V. Nazabal, and R. Lebullenger, “Glass formation in the Sb2O3-CdCl2-SrCl2 ternary system,” *J. Non. Cryst. Solids*, vol. 357, no. 15, pp. 2984–2988, 2011.

[20] V. Himamaheswara Rao, P. Syam Prasad, M. Mohan Babu, P.Venkateswara Rao, Luís F. Santos, G. Naga Raju and N. Veeraiah, "Luminescence properties of Sm3+ ions doped heavy metal oxide telluritetungstate-antimonate glasses," Ceramics International *Ceram. Int.*, vol. 43, no. 18, pp. 16467–16473, 2017.

[21] L. Yuliantini, M. Djamal, R. Hidayat, K. Boonin, J. Kaewkhao, and P. Yasaka, “ScienceDirect Luminescence and Judd-Ofelt analysis of Nd 3 + ion doped oxyfluoride boro-tellurite glass for near-infrared laser application,” *Mater. Today Proc.*, vol. 43, no. July 2018, pp. 2655–2662, 2021.

[22] K. U. Kumar, P. Babu, C. Basavapoornima, R. Praveena, D. S. Rani, and C. K. Jayasankar, “Physica B : Physics of Condensed Matter Spectroscopic properties of Nd 3 + -doped

boro-bismuth glasses for laser applications," *Phys. B Condens. Matter*, vol. 646, no. August, p. 414327, 2022.

[23] C. Madhukar Reddy, N. Vijaya, and B. Deva Prasad Raju, "NiR fluorescence studies of neodymium ions doped sodium fluoroborate glasses for 1.06 lm laser applications," *Spectrochim. Acta - Part A Mol. Biomol. Spectrosc.*, vol. 115, pp. 297–304, 2013.

[24] D. Umamaheswari, B. C. Jamalaiah, T. Sasikala, G. V. L. Reddy, and L. R. Moorthy, "Investigation on 1.07 μm laser emission in Nd3+-doped sodium fluoroborate glasses," *J. Rare Earths*, vol. 30, no. 5, pp. 413–417, 2012.

[25] G. H. Dieke, "Spectra and Energy Levels of Rare Earth Ions in Crystals.," 1968.

[26] W. B. Fowler and D. L. Dexter, "Relation between absorption and emission probabilities in luminescent centers in ionic solids," *Phys. Rev.*, vol. 128, no. 5, p. 2154, 1962.

[27] J. Schanda and M. Danyi, "Correlated color-temperature calculations in the CIE 1976 chromaticity diagram," *Color Res. Appl.*, vol. 2, no. 4, pp. 161–163, 1977.

[28] R. L. Smith and G. E. Sandly, "An accurate method of determining the hardness of metals, with particular reference to those of a high degree of hardness," *Proc. Inst. Mech. Eng.*, vol. 102, no. 1, pp. 623–641, 1922.

[29] V. Dimitrov and S. Sakka, "Electronic oxide polarizability and optical basicity of simple oxides. I," *J. Appl. Phys.*, vol. 79, no. 3, pp. 1736–1740, 1996.

[30] J. Tauc, "Optical properties and electronic structure of amorphous Ge and SiNo Title," *Mater. Res. Bull.*, vol. 3, no. 1, pp. 37–46, 1968.

[31] D. F. Swinehart, "The beer-lambert law," *J. Chem. Educ.*, vol. 39, no. 7, p. 333, 1962.

[32] W. T. Carnall, P. R. Fields, and K. Rajnak, "Spectral intensities of the trivalent lanthanides and actinides in solution. II. Pm3+, Sm3+, Eu3+, Gd3+, Tb3+, Dy3+, and Ho3+," *J. Chem. Phys.*, vol. 49, no. 10, pp. 4412–4423, 1968.

[33] K. R. W.T. Carnall, P.R. Fields, "Electronic energy levels in the trivalent lanthanide aquo ions. I. Pr3+, Nd3+, Pm3+, Sm3+, Dy3+, Ho3+, Er3+, and Tm3+," *J. Chem. Phys.*, vol. 49, no. 10, pp. 4424 – 4442, 1968.

[34] C. S. McCamy, "Correlated color temperature as an explicit function of chromaticity coordinates," *Color Res. Appl.*, vol. 17, no. 2, pp. 142–144, 1992.